© 2016. Published by The Company of Biologists Ltd | Development (2016) 143, 2160-2171 doi:10.1242/dev.132704

RESEARCH ARTICLE

Primary cilia maintain corneal epithelial homeostasis by regulation of the Notch signaling pathway

Laura Grisanti[1], Ekaterina Revenkova[1], Ronald E. Gordon[2] and Carlo Iomini[1,3,*]

ABSTRACT

Primary cilia have been linked to signaling pathways involved in cell proliferation, cell motility and cell polarity. Defects in ciliary function result in developmental abnormalities and multiple ciliopathies. Patients affected by severe ciliopathies, such as Meckel syndrome, present several ocular surface disease conditions of unclear pathogenesis. Here, we show that primary cilia are predominantly present on basal cells of the mouse corneal epithelium (CE) throughout development and in the adult. Conditional ablation of cilia in the CE leads to an increase in proliferation and vertical migration of basal corneal epithelial cells (CECs). A consequent increase in cell density of suprabasal layers results in a thicker than normal CE. Surprisingly, in cilia-deficient CE, cilia-mediated signaling pathways, including Hh and Wnt pathways, were not affected but the intensity of Notch signaling was severely diminished. Although Notch1 and Notch2 receptors were expressed normally, nuclear Notch1 intracellular domain (N1ICD) expression was severely reduced. Postnatal development analysis revealed that in cilia-deficient CECs downregulation of the Notch pathway precedes cell proliferation defects. Thus, we have uncovered a function of the primary cilium in maintaining homeostasis of the CE by balancing proliferation and vertical migration of basal CECs through modulation of Notch signaling.

KEY WORDS: Primary cilia, Cornea, Ocular surface, Notch signaling, Epithelium, Wound healing, Mouse

INTRODUCTION

The outermost layer of the cornea consists of a stratified non-keratinized pseudosquamous epithelium known as corneal epithelium (CE). Its highly ordered architecture must be precisely maintained during homeostasis and re-established upon mechanical lesions in order to ensure clear vision. During corneal maturation, the basal epithelium stratifies resulting in differentiated suprabasal layers (wing cells) and more superficial cells that are ultimately eliminated through exfoliation (Thoft and Friend, 1983). At homeostasis the CE undergoes intensive cell renewal. Limbal stem cells localized at the periphery of the cornea undergo slow cell cycle and generate a population of fast-dividing cells called transient amplifying cells (TACs) (Cotsarelis et al., 1989). TACs migrate towards the center of the cornea and populate the basal epithelium to replenish the loss of suprabasal cells that are exfoliating from the corneal surface (Cotsarelis et al., 1989; Davanger and Evensen, 1971). Despite this intense process of self-renewal, the overall mass, cell density, and architecture of the CE remain constant throughout adult life (Thoft and Friend, 1983). Imbalances between proliferation and differentiation of stem cells or TACs may cause corneal epithelial defects during development, homeostasis or repair (Douvaras et al., 2013; Huang et al., 1991; Nishida et al., 1995). However, how cell proliferation, migration and differentiation are integrated and regulated during corneal homeostasis and repair is not well understood.

Primary cilia are microtubule-based cellular organelles protruding from the surface of most eukaryotic cells. Cilia play crucial roles in signaling pathways that control morphogenesis, proliferation, polarity and differentiation during development and tissue homeostasis, such as the Hh, Wnt and Notch pathways (Berbari et al., 2009; Wood et al., 2013). A bidirectional movement of protein particles along the inner microtubular core, the axoneme, called intraflagellar transport (IFT) ensures the appropriate assembly and maintenance of cilia (Rosenbaum and Witman, 2002). Defects in ciliary proteins result in developmental abnormalities and lead to a large spectrum of syndromic diseases collectively referred to as ciliopathies (Goetz and Anderson, 2010; Sharma et al., 2008). Intriguingly, a description of a patient affected by Meckel syndrome, a severe ciliopathy, reported multiple conditions of the anterior segment including an unusual thickening of the cornea (MacRae et al., 1972). However, to date it is not known whether cells of the CE are ciliated and whether the cilium plays any role in the biology, formation, differentiation, development or organization of the CE.

In the skin, a tissue that shares similar embryonic origins, stratified organization and molecular signatures with the CE, primary cilia control hair follicle development and epidermis proliferation (Croyle et al., 2011). In addition, it was shown that disruption of IFT components diminishes Notch activity leading to compromised skin differentiation and barrier function (Ezratty et al., 2011). Notch signaling plays a key role in proliferation and differentiation of several tissues (Chen et al., 2014; Guentchev and McKay, 2006). Activation of the pathway occurs through the interaction of Notch ligands of the Delta-like and Jagged families with the receptors of the Notch family (Notch1-4). Ligand binding results in the cleavage of the Notch receptor at the membrane (Kopan and Ilagan, 2009; Schroeter et al., 1998) and the release of the Notch intracellular domain (NICD). The freed NICD translocates to the nucleus where it activates target genes such as those encoding the Hes and Hey transcription factors, which in turn affect numerous pathways involving cell fate determination. The involvement of primary cilium in the regulation of Notch pathway, however, is debated mostly owing to contradictory findings in ciliary mutants, ranging from inactivation to overactivation of the

[1]Department of Ophthalmology and Friedman Brain Institute, Icahn School of Medicine at Mount Sinai, One Gustave L. Levy Place, New York, NY 10029, USA. [2]Department of Pathology, Icahn School of Medicine at Mount Sinai, One Gustave L. Levy Place, New York, NY 10029, USA. [3]Department of Developmental and Regenerative Biology, Icahn School of Medicine at Mount Sinai, One Gustave L. Levy Place, New York, NY 10029, USA.

*Author for correspondence (carlo.iomini@mssm.edu)

C.I., 0000-0001-6483-9540

Received 11 November 2015; Accepted 11 April 2016

Development (2016) 143, 2160-2171 doi:10.1242/dev.132704

pathways (Cervantes et al., 2010; Ezratty et al., 2011; Leitch et al., 2014; Liu et al., 2014).

Interestingly, in the ocular surface Notch activation contributes to the maintenance of the stratified and non-keratinized corneal and conjunctival cells differentiation and function (Djalilian et al., 2008; Ma et al., 2011; Nakamura et al., 2008; Vauclair et al., 2007; Xiong et al., 2011; Zhang et al., 2013). This led us to hypothesize that primary cilia could play an important role in maintaining CE homeostasis and/or morphogenesis.

In this study, we have investigated the role of primary cilia during development, adult homeostasis and repair of the CE. We show that ciliated cells are mostly present at the basal layer of the CE and establish a strong correlation between full differentiation commitment of basal CECs and cilia disassembly with basal bodies disengagement from the apical membrane. We demonstrate that, differently from other tissues of the ocular surface, cilia formation is not required for early stages of CE repair involving cell migration. Rather, corneal epithelial cilia appear to play an important role in balancing cell proliferation and differentiation at homeostasis and, thus, in maintaining constant thickness and architecture of the CE in adult life. We also show that ablation of epithelial cilia diminishes Notch pathway activity before leading to abnormal hyperproliferation of basal CECs. Furthermore, we propose that in the CE, primary cilia play a role in maintaining basal cells in an undifferentiated state establishing a balance between proliferation and differentiation through the regulation of the Notch pathway activity.

RESULTS

Ciliated cells are restricted to the basal corneal epithelium

In the mouse, CE forms at embryonic day (E) 11-12 from the external surface ectoderm after the lens vesicle separates from it. At this stage, the CE consists of a two-cell-layered tissue with basal cuboid cells and superficial squamous cells. Bona fide stratification occurs during late gestation and continues throughout postnatal development until adulthood (Pei and Rhodin, 1971).

To investigate the spatiotemporal dynamics of assembly/disassembly of primary cilia in the corneal epithelium, we analyzed the ocular surface in mice of different developmental ages by immunofluorescence and transmission electron microscopy (TEM). Primary cilia were identified using antibodies specific for acetylated α-tubulin and γ-tubulin, which are major components of the ciliary axoneme and the basal body (bb), respectively. Between E12.5 and E17.5 we found primary cilia protruding from the apical surface of the majority of basal cells (Fig. 1A) and, infrequently, from a subset of suprabasal cells (Fig. 1Ai-iii and Fig. 1B upper panel). By E17.5 though, when the epithelium begins to stratify, primary cilia were observed almost exclusively on the apical surface of basal cells (Fig. 1Aiv,v) and were absent in the most superficial cells (Fig. 1Avi and Fig. 1B lower panel). During postnatal corneal development and in adult cornea, cilia were detected exclusively at the apical side of basal cells (Fig. 1C). Quantification analysis of central and peripheral CE (Fig. 1D) indicated that overall the number of ciliated cells in the corneal epithelium progressively decreased during development changing from ∼90% during gestation to only ∼30% in the adult (Fig. 1E). The decrease was particularly strong in the postnatal day (P) 10-20 interval (Fig. 1E), when the eyelids open and the CE undergoes important morphogenetic changes (Zieske, 2004). Although we did not detect differences in density of ciliated cells at the center or periphery of the CE, peripheral cells had longer cilia (Fig. 1F).

Apico-basal TEM sections of the CE confirmed the localization of cilia projecting from the apical membrane of basal CEC toward the suprabasal layers (Fig. 1G-M). Furthermore, in both embryos and adult animals the ciliary tip interacted with the plasma membrane of suprabasal cells, whereas the proximal region of CEC cilia was partially invaginated in the ciliary pocket (Fig. 1I,K). However, in some basal cells of the adult, cilia appeared almost entirely invaginated in the ciliary pocket with limited contact with the cell membrane of suprabasal cells (Fig. 1L). Interestingly, in the adult, bbs of non-ciliated basal cells maintained contact with the apical cell membrane (Fig. 1M, lower panel). By contrast, in both adult and embryos, the bbs of suprabasal cells were always found to be disengaged from the apical membrane and lacking cilia (Fig. 1J-M upper panel). Overall, our ultrastructural analysis suggests that during homeostasis loss of cilia occurs before vertical movement of the basal CECs towards the corneal surface.

Primary cilia ablation results in abnormal CE cell proliferation and stratal thickness

To elucidate the function of primary cilia in the CE, we conditionally targeted *Ift88* in CECs by crossing mice with floxed *Ift88* allele (*Ift88*^{fl}) (Haycraft et al., 2007) with *K14*^{Cre} transgenic line. In these mice (*K14Ift88* cKOs), the Cre expression is driven by the *K14* (*Krt14* – Mouse Genome Informatics) promoter, which is active by E14-15 in basal undifferentiated cells of the CE (Kurpakus et al., 1994; Tanifuji-Terai et al., 2006). To monitor Cre activity, we utilized the *Rosa26*$^{mT/mG}$ reporter line (Fig. 2A) (Muzumdar et al., 2007), in which the Cre-dependent excision of a cassette expressing the red fluorescent membrane-targeted tdTomato (mT) allows the expression of a membrane-targeted green fluorescent protein (mG). Cre expression was confirmed in nearly all basal CECs of adult mice (Fig. S1A) and the depletion of *Ift88* mRNA and Ift88 protein in the CE of *K14Ift88* cKOs was corroborated by RT-PCR and western blot, respectively (Fig. S1B,C). Although we occasionally detected cilia in basal CECs of newborn mutant mice, cilia were never observed in CECs of P13 or older mice (Fig. S1D,E). Although corneas from both mutant and control adult (3 months) mice were transparent by slit lamp evaluation (Fig. 2B), the central CE of mutant mice displayed an increase in thickness of ∼20% compared with control, as assessed by plastic and paraffin sections (Fig. 2C-E; Fig. S1F), with the largest difference in thickness detected at the center of the CE and the lowest in the limbal region located at the cornea periphery (Fig. 2D; Fig. S1F). The corneas of older mutant mice (11 months) remained transparent (Fig. S1G) and displayed a similar increase in central epithelial thickness (Fig. 2E; Fig. S1H). Other corneal tissues of the *K14Ift88* cKOs, including stroma and endothelium, were indistinguishable from those of the control (Fig. 2C; Fig. S1F). Ultrastructural analysis confirmed the abnormal thickening of the CE and revealed disorganization of suprabasal cell layers. Wing cells appeared more numerous in the mutant than in control corneas (Fig. 2F). To quantify differences in CEC density in living tissue, we compared corneas from adult mutant and control animals carrying the mT/mG cassette using *ex vivo* confocal imaging. Membrane-targeted GFP and tdTomato allowed clear identification of cell outlines in different layers of the CE (Fig. 2G). The cell density of basal CE (expressed as number of cells in a given area) was similar in both mutant and control mice (Fig. 2H′). By contrast, the cell density of suprabasal cells (expressed as ratio of suprabasal cells/basal cells in a given area) was 20% higher in the mutant than in the control (Fig. 2H).

The abnormally elevated density of suprabasal cells detected in the mutant could result from the atypical proliferation of suprabasal cells and/or from the hyperproliferation of the basal layer cells matched by an equivalent increase in the stratification rates. To distinguish between these two possibilities, we performed

Development (2016) 143, 2160-2171 doi:10.1242/dev.132704

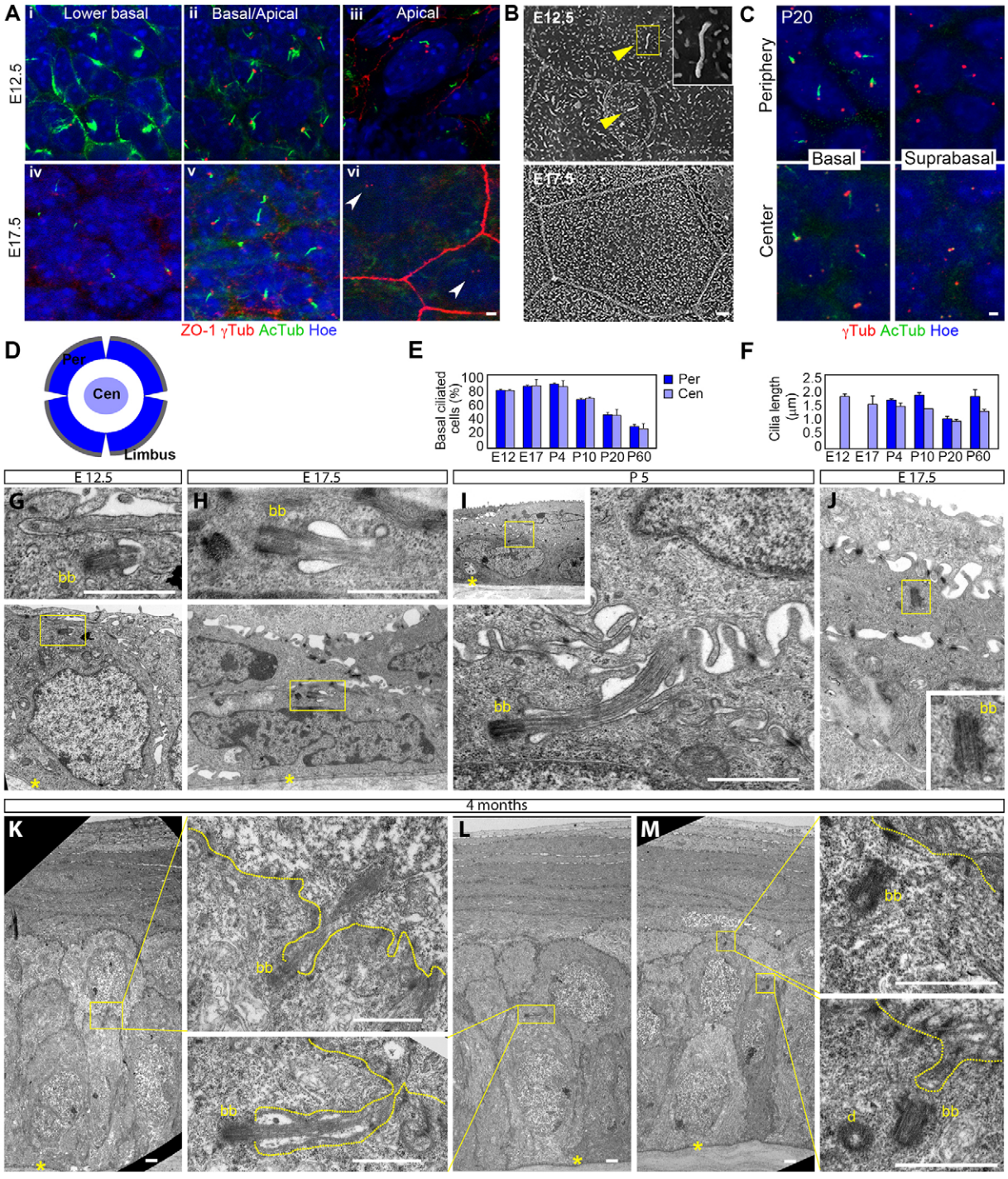

Fig. 1. Primary cilia of CECs disassemble during postnatal development. (A) Confocal images of whole-mounted corneas at E12.5 (i-iii) and E17.5 (iv-vi). Cilia are stained for acetylated tubulin (green), basal bodies for γ-tubulin and apical cell membranes for ZO-1 (both in red). Hoechst 33342 stains nuclei in blue. Arrowheads indicate basal bodies without cilia. (B) SEM images show the presence of cilia (yellow arrowheads) on the superficial cells of the CE at E12.5 and their absence at E17.5. (C) By P20, ciliated CECs are only found at the basal layer. (D) Random microscope fields were taken in a peripheral annulus ∼250 µm wide (not including limbus) and a central circle of ∼250 µm diameter. (E,F) Percentage of ciliated cells in the basal CE (E) and cilia length (F) at different developmental ages (>100 cilia/bb were counted for each animal; number of animals n=2 for each group). Results are mean±s.d. (G-M) TEM images of the CE cilium and bb during development and in adult stages. Plastic sections were cut perpendicularly to the basement membrane. Dotted lines outline apical membrane in adult CE. Boxed areas are shown at higher magnification. Asterisks indicate basement membrane. d, daughter centriole. Scale bars: 1 µm.

bromodeoxyuridine (BrdU) pulse experiments in adult *K14Ift88* cKO mice and analyzed flat-mounted corneas by confocal microscopy. To assess cell proliferation in the CE of adult mice, we quantified BrdU-positive cells 2 h after BrdU administration (Fig. 3A,B). Although proliferative cells were present at the basal epithelium, they were absent or scarce in the suprabasal epithelium of both *K14Ift88* cKO and control mice (Fig. 3A,B). However, the percentage of BrdU-positive cells in the basal CE of the *K14Ift88* cKO adult mice was nearly double that of control mice both at the periphery and at the center of the cornea (Fig. 3A,B). Similar results

Development (2016) 143, 2160-2171 doi:10.1242/dev.132704

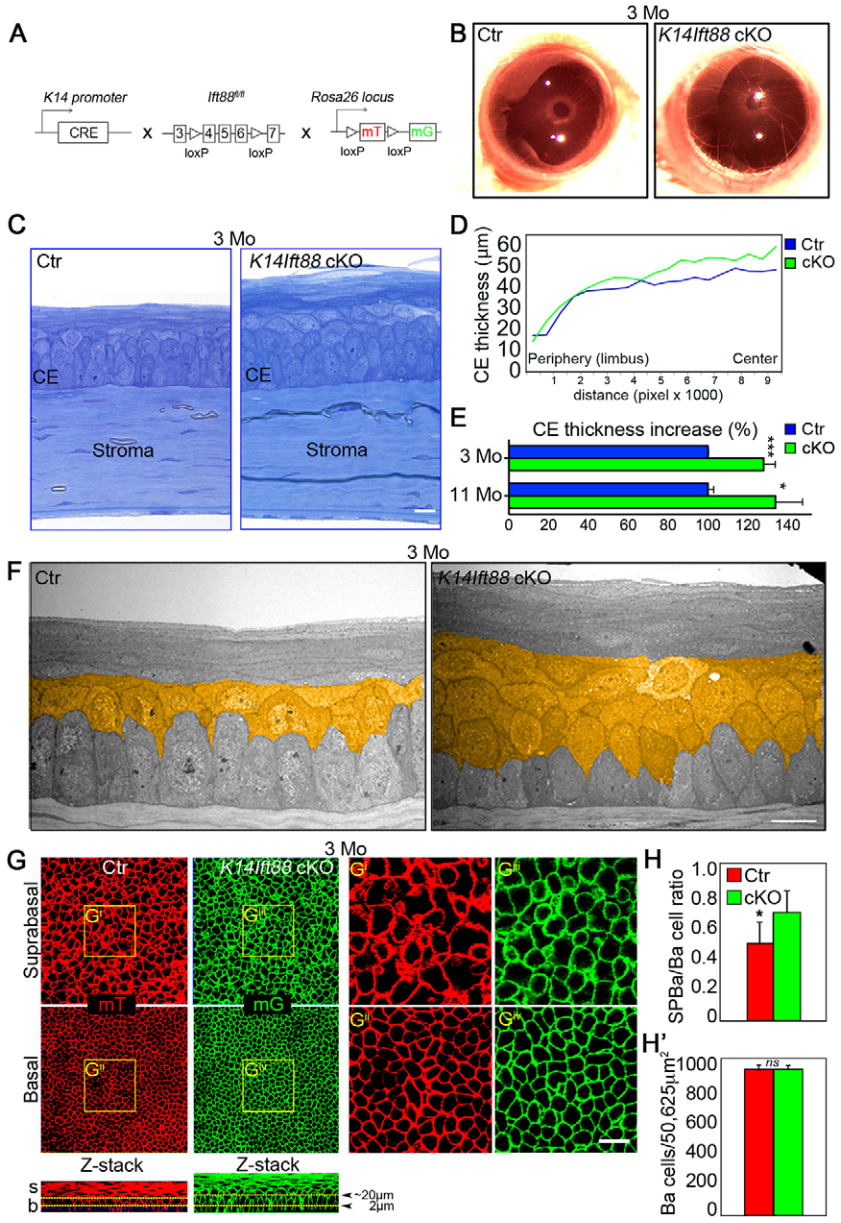

Fig. 2. Ablation of Ift88 induces accumulation of CECs in the suprabasal layer and abnormal CE thickening. (A) Schematic of cross strategy to generate *K14Ift88* cKO animals (*K14^{cre};Ift88$^{fl/fl}$*) with reporter line *R26$^{mT/mG}$*. (B) Corneas of control and *K14Ift88* cKO mice look normal and transparent. (C) Toluidine Blue staining of control and *K14Ift88* cKO Epon-embedded corneas on sagittal thin sections showing a thicker CE in the mutant. (D) The thickness of the epithelium along the cornea in *K14Ift88* cKOs is represented by the green line compared with control (blue line) in a representative experiment (one cornea embedded in plastic and partially displayed in panel C). (E) Thickness of *K14Ift88* cKO corneal epithelium normalized to control. Results are mean±s.d. (number of animals in 3- and 11-month-old groups were n=4 and n=2, respectively; two cornea for each animal were analyzed). *P<0.05, ***P<0.001; Student's t-test. (F) TEM image of central CE of adult *K14Ift88* cKO (right panel) clearly reveals the accumulation of epithelial cells in the immediate suprabasal layer compared with that of control corneas (left panel). Yellow highlights indicate suprabasal cells confined between basal and superficial cell layers. (G) *Ex vivo* confocal images show the suprabasal and basal layers of control cornea (*IFT88$^{fl/fl}$;R26$^{mT/mG}$*) in red and *K14Ift88* cKO cornea (*K14^{Cre};IFT88$^{fl/fl}$;R26$^{mT/mG}$*) in green. The bottom panels show the z-sections of the epithelium in both control and *Ift88* mutant mice. Yellow dotted lines indicate suprabasal (s) and basal (b) sections analyzed in the upper images. Distance from the basal lamina is indicated. (Gi-Giv) Areas within the yellow boxes in G are shown at higher magnification. (H,H′) The absolute number of basal (Ba) cells is similar in both control and *K14Ift88* cKO mice as shown in the bottom graph. However, the top graph shows the increased number of suprabasal (SPBa) cells in the *Ift88* mutant. This difference is represented by the ratios between suprabasal and basal epithelial cells in control and *K14Ift88* cKO corneas. Results represent mean±s.d. (number of animals in each group n=2, one cornea per animal was analyzed). *P<0.05; ns, non-significant; Student's t-test. Mo, months. Scale bars: 10 µm.

were also obtained by immunostaining of phosphohistone H3 (PHH3), a marker for mitotic nuclei (Fig. 3C). Given that cell density of the basal cell layer is similar in both mutant and control animals, we expected that the number of basal cells migrating towards the suprabasal compartment per unit of time (rate of vertical cell migration) would be higher in the mutant than in the control. To quantify this process, we sacrificed mice at 18, 24 and 72 h after a single BrdU injection and quantified BrdU-positive cells at the basal and suprabasal layers of central CE (Fig. 3D-F). As expected, the percentage of BrdU-positive cells in the suprabasal layer was significantly higher in *K14Ift88* cKOs than in control mice. However, the loss of BrdU-positive cells at the basal CE occurred more rapidly in the mutant than in the control (Fig. 3F). Taken together, these results indicate higher rates of vertical cell migration in the CE of mutant mice. Thus, these data suggest that ablation of primary cilia in the CE leads to basal CEC hyperproliferation in conjunction with elevated rates of vertical cell migration, resulting in the disorganization of the suprabasal CEC (wing cells) compartment and abnormal corneal thickening in adult mutant mice.

Primary cilia are not required for CE wound closure

Corneal epithelial injury repair is a multistep process involving cell motility and proliferation. First, CECs near the injury disassemble anchoring structures, flatten and migrate as an intact sheet to cover the wound. Then, cells distal to the wound proliferate to compensate for cell loss at the wounded area, and cell stratification and differentiation occurs (Zagon et al., 1999). Typically, in mice a mechanical wound of ∼1.5 mm in diameter completely closes in ∼24 h (Stepp et al., 2014). To address cilia dynamics and function during CE repair, we performed a central epithelial injury and followed cilia assembly/disassembly in CECs located proximally (central CEC) or distally (peripheral CEC) to the wound at different time points following the lesion. Surprisingly, shortly after wounding (6 to 18 h) cilia completely disassembled in the large majority of central CECs neighboring the wound (Fig. 4A). By contrast, at the periphery the percentage of ciliated CECs remained unchanged and the ciliary length increased by ∼20% compared with that of corresponding cells in control intact CE (Fig. 4B-C′). Central CECs progressively reassembled cilia only 24 h following injury,

Development (2016) 143, 2160-2171 doi:10.1242/dev.132704

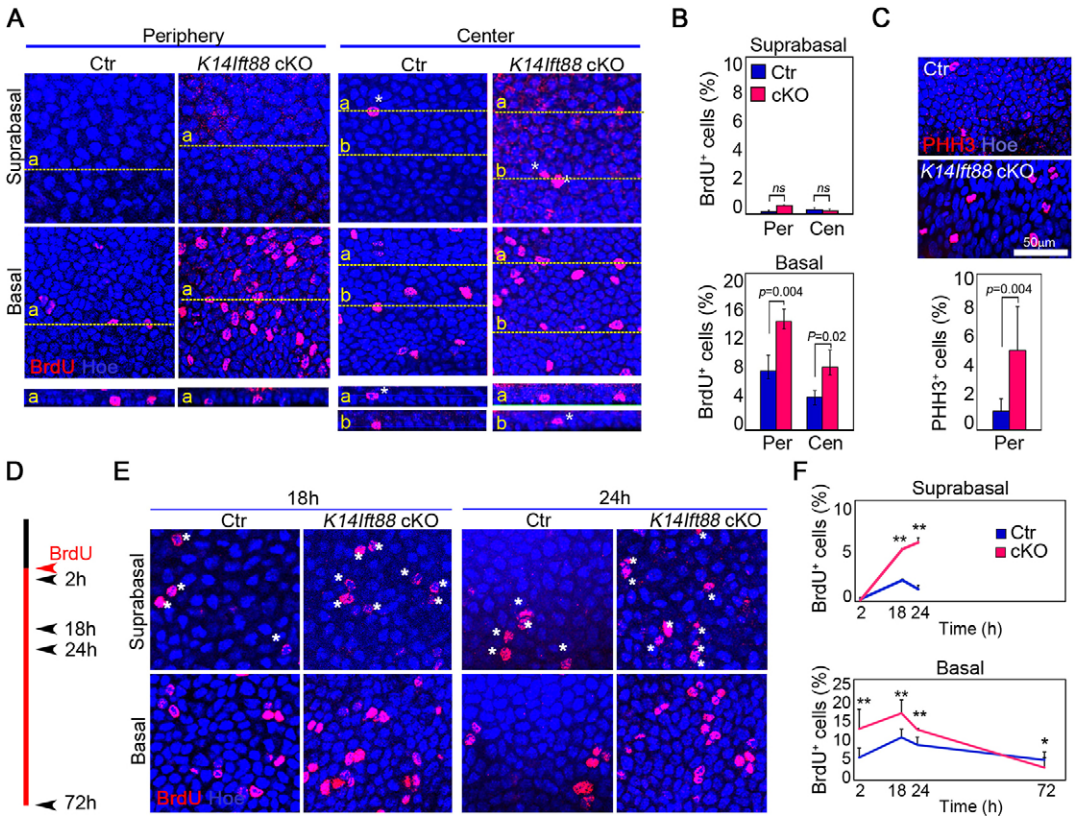

Fig. 3. Proliferation and basal-to-apical migration of CECs in *K14Ift88* cKO and control mice. (A) BrdU staining of whole-mounted corneas 2 h after BrdU administration in control and *K14Ift88* cKO mice. Corresponding single optical sections of suprabasal and basal cell layers in the periphery and center of control and *K14Ift88* cKO mice are shown. Yellow dotted lines indicate the position of the orthogonal projections showed at the bottom of each panel. Occasional BrdU-positive cells in the suprabasal layers are indicated by a white asterisk. (B) BrdU-labeling index in control and *K14Ift88* cKO corneas (number of animals in each group n=4). (C) Mitotic marker PHH3 staining and quantification of proliferating cells in control and *K14Ift88* cKO mice (n=3). (D) BrdU was administered to animals 2, 18, 24 and 72 h prior to each analysis to follow the fate of labeled cells. (E) Staining for BrdU on whole-mounted corneas at different time points shows increased number of labeled cells (white asterisks) in the suprabasal compartment of *K14Ift88* cKO epithelium. (F) Increase of BrdU-positive suprabasal cells (upper panel) and loss of BrdU-positive basal cells (lower panel) in *K14Ift88* cKO and control central corneas (number of animals in each group n=2). In B,C,F, data represent the mean percentage of BrdU-positive or PHH3-positive cells in relation to total basal epithelial cells. *P<0.05, **P<0.01; ns, non-significant $P\geq0.05$; Student's t-test. Cen, central; Per, peripheral.

which approximately coincided with complete wound closure (Fig. 4C). Ciliated cell density at the center and ciliary length of the peripheral cells reverted to values found in intact corneas ∼48 h post-injury, thus coinciding with the re-establishment of normal CEC stratification, differentiation and exfoliation (Fig. 4B,C). To determine whether absence of Ift88 affects the process of CE wound healing, we performed a 1.5-mm epithelial abrasion and followed the wound closure by fluorescein staining. In a typical experiment, epithelial wound recovery occurred within 24 h in corneas from both *K14Ift88* cKO and control mice (n=3) (Fig. 4D). Although complete re-epithelialization and re-establishment of normal CE architecture requires proliferation, the initial phase of wound closure is independent of cell division (Friedenwald and Buschke, 1944; Kuwabara et al., 1976; Zagon et al., 1999). During the initial phase of cornea re-epithelialization upon a central mechanical wound, cell proliferation rates drastically decrease in cells proximal to the wound borders. By contrast, they increase at the cornea periphery distally to the wound and reach a peak 24 h after wounding (Stepp et al., 2002). Because *Ift88* ablation leads to hyperproliferation in the basal CE, we investigated whether proliferation rates were altered in the healing *K14Ift88* cKO CE. A 1.5-mm wound was produced in the cornea of wild-type (WT) and *K14Ift88* cKO animals and BrdU was administered 2 h prior to the analysis of the center and periphery of the CE at 18, 24, 48 and 72 h (Fig. 4E). Surprisingly, we found a similar increase in BrdU-positive cells at the periphery of both *K14Ift88* cKO and control mice (from ∼5% to ∼30%), although in the mutant the peak of proliferation during healing was reached 6 h earlier than in the control (Fig. 4F). We did not detect any BrdU-positive cells near the wound margin at the center of the cornea at any time post-wounding (up to 18 h) in both cKO and control (Fig. 4F′).

Overall, these results indicate no changes in wound closure speed and in cell proliferation rates of the mutant CECs during repair, suggesting that the cilium is not required during an early response in CE repair and that during repair cell proliferation is controlled independently from the cilium.

Ablation of Ift88 reduces Notch pathway activity in the CE

Hh, and more unpredictably Wnt and Notch, pathways have been linked to ciliary function. We therefore used quantitative real-time PCR (RT-qPCR) and reporter mouse lines to examine the expression of specific Hh, Wnt and Notch target genes in CE. Surprisingly, expression profiles of genes controlled by Hh and Wnt pathways were indistinguishable between *K14Ift88* cKO and control mice (Fig. 5A). Moreover, reporter mice for Wnt and Shh pathways revealed no detectable activation of these pathways in the CE during cornea development (Fig. S2). By contrast, Notch target genes, including *Hey1*, *Hes1* and *Maml1*, were all downregulated in the *K14Ift88* cKO CE compared with control (Fig. 5A).

Development (2016) 143, 2160-2171 doi:10.1242/dev.132704

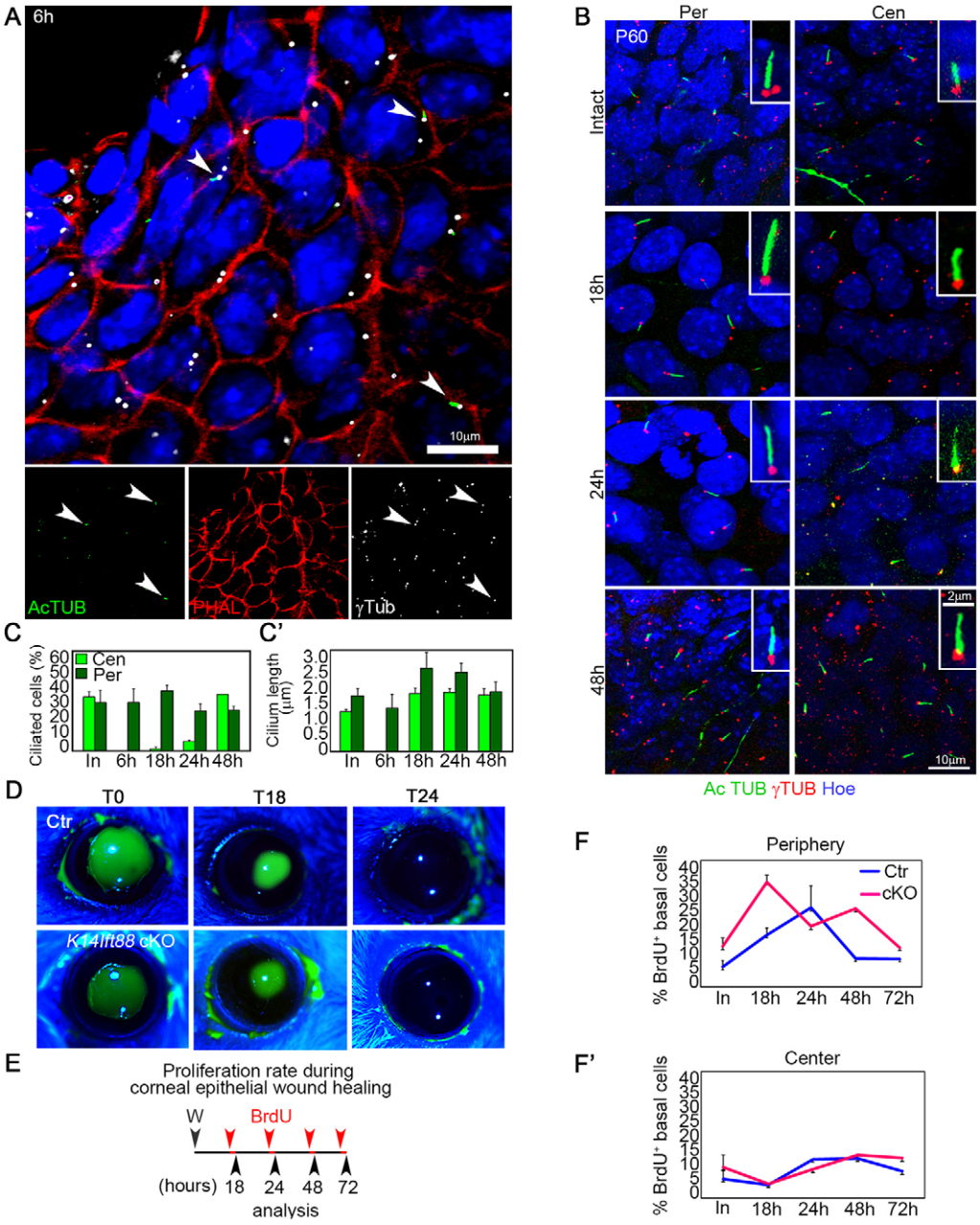

Fig. 4. Ciliary loss does not affect corneal epithelial wound healing process. (A) Immunofluorescence staining for α-tubulin (green), γ-tubulin (white) and phalloidin (red) on wild-type corneal buttons 6 h after central cornea debridement. Note that epithelial cells neighboring the leading edge of the wound lack cilia during the healing process. Arrowheads indicate occasional ciliated CECs. (B) Ciliogenesis occurring during and post wound closure in peripheral and central cornea. Insets show higher magnification of primary cilia. (C,C′) Quantification of cilia (expressed as percentage of ciliated cells relative to the total bb number) and their length during wound healing in peripheral and central corneas. In C, values were compared between center and periphery at each time point. In C′, all values for center were compared with center intact; all values for periphery were compared with periphery intact (number of animals in each group n=2). (D) Mechanical removal of 1.5 mm of central corneal epithelium in control and *K14Ift88* cKO mice. By 24 h after debridement (T24), the epithelium is completely healed in both animals as shown by the absence of fluorescein staining (number of animals in each group n=3). (E) Schematic of BrdU experiments during the wound-healing process. BrdU was administered 2 h before sacrificing each group of animals 18, 24, 48 or 72 h after wounding. (F,F′) The proliferation rate of epithelial basal cells at the periphery (F) and at the center (F′) during cornea regeneration. In C,C′,F,F′, results represent mean±s.d. *P<0.05, **P<0.01, ***P<0.001; two-way ANOVA with Bonferroni post-tests for pairwise comparisons. Cen, central; Per, peripheral.

To understand the role of Ift88 in the Notch pathway, we first analyzed Ift88-deficient cells for the presence of Notch1 intracellular domain (N1ICD), which is responsible for the transcriptional activation of Notch-regulated genes. We detected N1ICD staining in 80% of the nuclei of control CE. By contrast, only 20% of the nuclei were N1ICD positive in the CE of *K14Ift88* cKO (Fig. 5B,C). Of note, in both mutant and control CE we only detected N1ICD in the nuclei of basal and suprabasal CECs but not in superficial CECs (Fig. 5B,B′). Western blot analysis of isolated CE showed a lower level of N1ICD in the *K14Ift88* cKO compared with control CECs (Fig. 5D). As N1ICD is a proteolytic product of Notch1, the reduction of N1ICD-positive nuclei in the CE of the *K14Ift88* cKO could be due to low levels of the Notch1 receptor in the mutant tissue. To test this possibility, we analyzed the localization and expression of the Notch1 receptor. Notch1 immunofluorescence at the basal and suprabasal cell layers generated similar signals in both *K14Ift88* cKO and control CE (Fig. 5E) paralleling the indistinguishable *Notch1* and *Notch2* transcriptional profile and protein expression levels in the mutant and control CE (Fig. 5F,G). Taken together, these results suggest that Ift88, and possibly the CE primary cilium, function downstream of the activation of the Notch1 receptor and act as a positive regulator of the Notch pathway by maintaining normal levels of N1ICD.

Next, we investigated whether there was a direct association between Notch activity and cell proliferation in basal CECs at homeostasis. We performed double staining with antibodies directed to BrdU and N1ICD on frozen sections of corneas from WT and *K14Ift88* cKO adult mice sacrificed 2 h after BrdU administration (Fig. 6A,B). We found that the percentage of BrdU-positive cells in the N1ICD-negative population was 23.0% in the WT and 14.1% in the mutant. By contrast, in the N1ICD-positive population, the percentage of BrdU-positive cells was only 5.3% in the WT and 6.9% in the mutant (Fig. 6C). Thus, nuclear translocation of the N1ICD in basal CECs is associated with a decrease in proliferation rates.

Development (2016) 143, 2160-2171 doi:10.1242/dev.132704

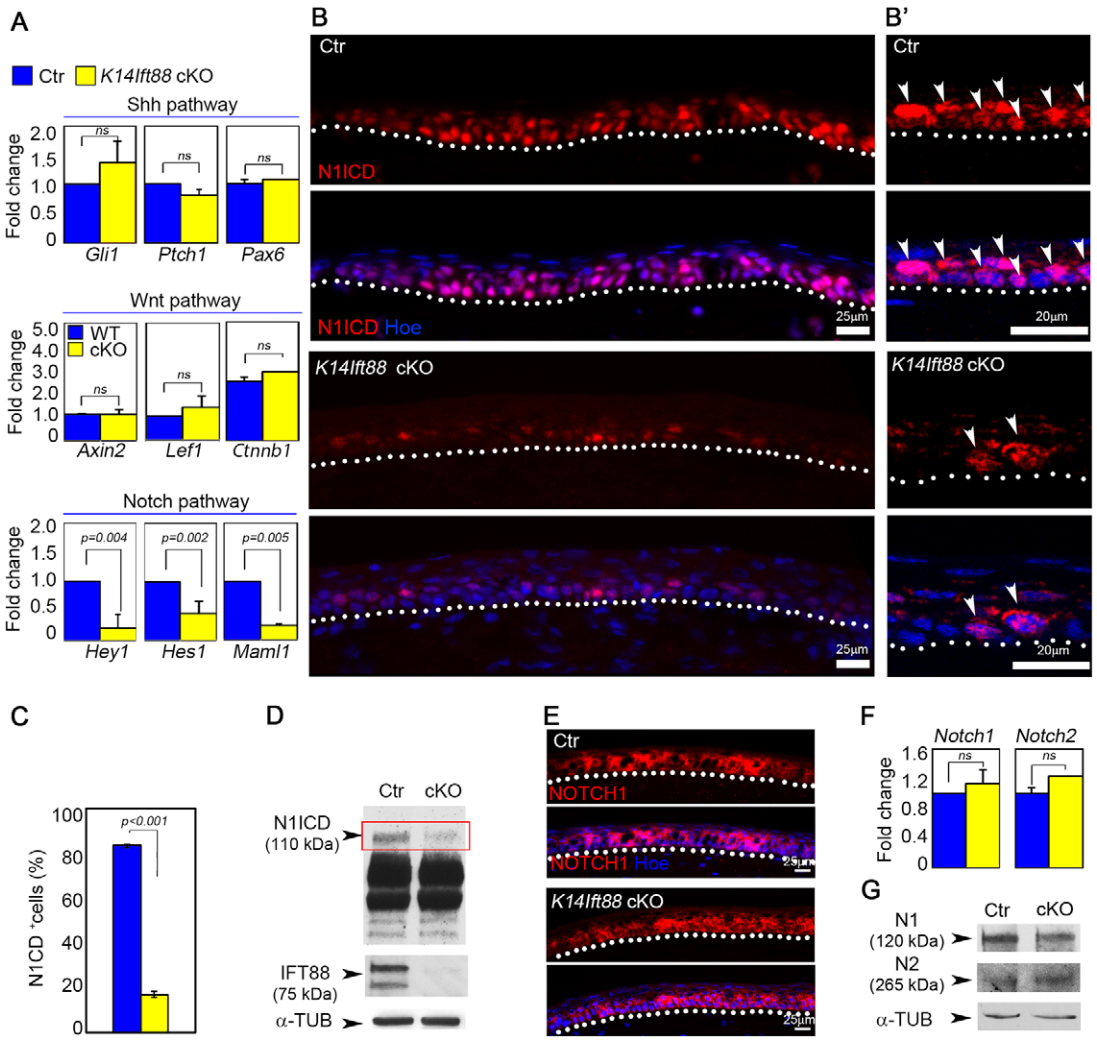

Fig. 5. Notch1 signaling activity decreases in *K14Ift88* cKO corneal epithelium. (A) qRT-PCR analysis of Shh, Wnt and Notch target genes in isolated CE shows significant downregulation of the Notch1 target genes *Hey1*, *Hes1* and *Maml1* expression in mutant tissue (number of animals in each group *n*=2). (B) Immunofluorescence for Notch1 intracellular domain (N1ICD) on control and *K14Ift88* cKO corneal sections. (B′) Confocal images show the nuclear localization of N1ICD in basal and suprabasal cells of the corneal epithelium. Note the reduced nuclear staining in *K14Ift88* cKO compared with the control corneas (arrowheads). (C) Quantification of N1ICD-positive cells in *K14Ift88* cKO corneas (number of animals in each group *n*=3). (D) Western blot for N1ICD (red box) and Ift88 on isolated epithelial cells from WT and *K14Ift88* cKO mice. (E-G) Notch1 and Notch2 staining in *K14Ift88* cKO corneas reveals no difference in protein expression, confirmed by qRT-PCR (F) and western blot (G). Corneas were from 3-month-old mice. Data are mean±s.d. ns, non-significant. Student's *t*-test. Dotted lines in B,B′,E indicate the basement membrane.

Decreased activity of Notch signaling precedes proliferation defects in *Ift88* conditional mutants

During postnatal mouse development, CE proliferation rates steadily increase during the first week of life peaking around P7-10 and beginning to decline prior to the eyelid opening at P12-15 (Tseng et al., 1999). Interestingly, it was reported that Notch activity, assessed by N1ICD staining, becomes detectable in basal and suprabasal CECs around P10 and appears more intense at P90 (Djalilian et al., 2008). Therefore, the time frame between P10 and P15 represents a crucial developmental stage at which Notch activity increases and proliferation rates decline towards the homeostatic levels observed in adult mice. We reasoned that this transitional stage of CE development could allow us to determine whether the ablation of *Ift88* impacts Notch activation or proliferation first. Although we detected occasional CE cilia at birth, complete cilia ablation was achieved by P13 in the CE of *K14Ift88* cKO (Fig. S1). Importantly, in both control and mutant mice the opening of the eyelid occurred at P13; however, in the mutant it was completed at P14 (Fig. 7A). Consistent with previous data (Tseng et al., 1999), we found that proliferation rates of basal CECs (assessed as percentage of BrdU-positive CECs at the cornea center and periphery) were high (16-18%) at P9 but decreased to 7-9% at P13 in both control and mutant mice (Fig. 7B). By contrast, at P15 whereas proliferation rates of basal CECs continued to decrease (~5%) in the control, they were increasing in the mutant (14%) (Fig. 7B). When we assessed Notch activation by N1ICD staining, we observed that at P13 the number of N1CID-positive cells in the *Ift88* cKO mutant was 50% lower than in control animals (Fig. 7C,D).

These results showed that during the postnatal development of CE up to P13 the ablation of primary cilia decreases Notch signaling, but does not alter proliferation rates of CECs, supporting the notion that primary cilia of the CE regulate the Notch pathway independently of cell division.

Development (2016) 143, 2160-2171 doi:10.1242/dev.132704

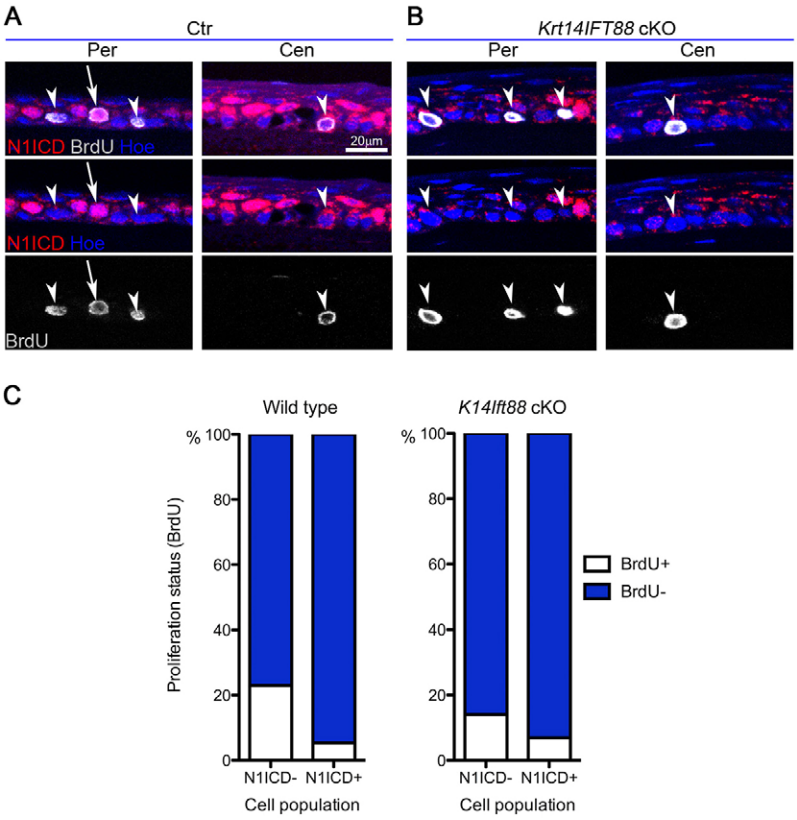

Fig. 6. Proliferation rate is low in basal CECs with an active Notch pathway. (A,B) N1ICD and BrdU staining on control and *K14Ift88* cKO corneas 2 h after BrdU administration. Arrowheads indicate N1ICD-negative cells that are BrdU positive. Arrows indicate double-positive cells.
(C) Quantification of N1ICD-positive and N1ICD-negative basal cells exhibiting or lacking BrdU staining in adult corneal epithelia of control and *K14Ift88* cKO. Difference in the proportions of BrdU-positive cells between N1ICD-positive and N1ICD-negative cell populations is statistically significant both for wild-type and *K14Ift88* cKO mice. Fisher's exact test, $P<0.0001$ (total number of cells 261) and $P=0.037$ (total number of cells 443), respectively. Number of animals for each genotype $n=4$. Cen, central; Per, peripheral.

DISCUSSION

In this study, we uncovered a novel role of primary cilia in maintaining homeostasis of the CE. We showed that corneal epithelial cilia protrude from the apical membrane of most basal CECs and that cilia ablation is associated with the thickening of the CE. Our findings demonstrate that conditional depletion of Ift88 in the CE leads to ablation of cilia, reduction of the Notch pathway activation, increased cell proliferation and upwards cell migration, which in turn results in an abnormally thick CE.

Primary cilia disassembly and bb undocking from the apical membrane correlates with basal cell commitment to terminal differentiation

We showed for the first time the spatiotemporal dynamics of cilia assembly/disassembly in mouse CE. Ciliated cells appear to be confined to the basal cell layer and decrease in number during development. In adult mice, only ∼30% of basal CECs display a cilium and these cells appeared to be distributed with no obvious segregation throughout the entire CE. Nevertheless, cilia of peripheral CECs were significantly longer than cilia of central CECs. However, owing to the lack of accepted cell-specific markers, we cannot conclude whether or not limbal stem cells are ciliated. In addition, as we detected cilia by immunocytochemistry on fixed corneas, we cannot establish whether ciliated cells in adult CE represent a steady subpopulation or whether all basal CECs maintain the ability to assemble and disassemble cilia following a precise program or cycle before becoming terminally committed. Our TEM analysis showed that bbs of non-ciliated basal CECs maintain contact with the apical membrane, an important requirement for the initiation of ciliogenesis (Park et al., 2008; Schmidt et al., 2012). By contrast, in terminally differentiated suprabasal cells that lack cilia, bbs were always found in the cytoplasm completely disengaged from the apical membrane, suggesting that in these cells the ciliogenesis program is abolished. These findings uncover an intriguing correlation between cilia disassembly, bb position and cell differentiation in stratified epithelia pointing to the possibility that non-ciliated basal cells are primed to move upwards and repopulate the suprabasal layer. Consistent with this idea, in the epidermis ciliated cells were found mostly at the basal layer, whereas progressively fewer ciliated cells were observed in the spinous layer. Further investigation using live-cell microscopy will be required to determine possible relationships between cilia and CEC stratification.

Corneal thickening and proliferation

We showed that inactivation of the *Ift88* gene in K14-positive basal CECs leads to an abnormal and progressive thickening of the CE in mice. Although the inactivation of *Ift88* induced hyperproliferation of the basal CECs, it did not perturb their density or alter the post-mitotic status of suprabasal cells (Figs 2 and 3). CE thickening is caused by higher numbers of cell layers and density in the suprabasal compartment that result from the abnormal increase of proliferation and upwards migration of CECs from the basal layer. Similarly, in the skin epidermis depletion of *Ift88* led to hyperplasia of the basal layer but not of the granular, spinous and stratum corneum (Croyle et al., 2011; Ezratty et al., 2011). However, the basal layer of the epidermis, unlike the CE, displayed an abnormal expansion in the number of cell layers expressing keratin 5, a marker of basal cells (Croyle et al., 2011). This difference could reflect tissue-specific mechanisms in place during the stratification/differentiation processes of CE and skin epidermis.

The role of primary cilia and IFT proteins in the cell cycle is not well understood. *In vitro* results showing that depletion of Ift88 promotes cell cycle progression and increases rates of cell division

Development (2016) 143, 2160-2171 doi:10.1242/dev.132704

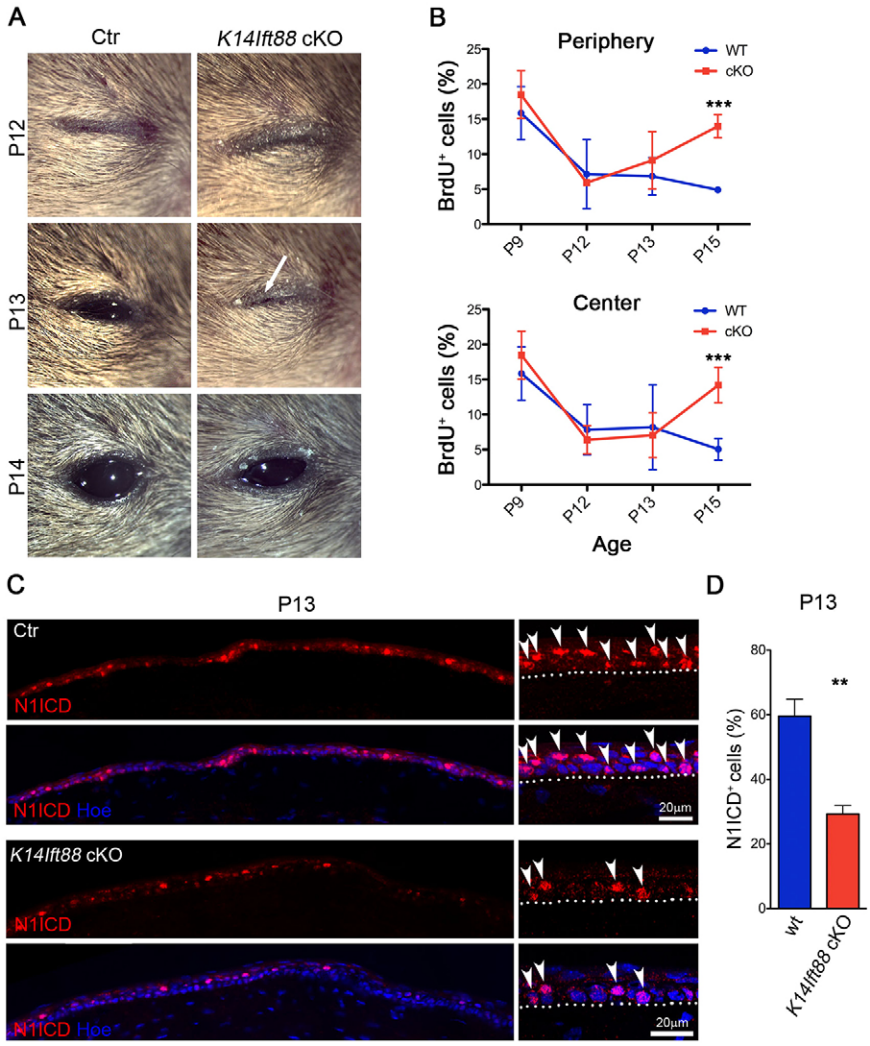

Fig. 7. N1ICD activity, but not cell cycle, is affected by ciliary loss during postnatal development of corneal epithelium in *Ift88* mutants. (A) Although eyelid opening occurs at P13 in both control and *K14Ift88* cKO mice, it is partial (arrow indicates beginning of the fissure) in the mutant. (B) Quantification of proliferating cells labeled with BrdU at different ages in both control and mutant mice in the peripheral and central corneas. For counts at P9, central and peripheral areas were not separated. Mice were sacrificed 2 h after BrdU injection (number of animals in each genotype $n \geq 2$). (C) Immunostaining for N1ICD on frozen corneal sections of P13 mice shows reduction of N1ICD expression in the CE of the mutant. Arrowheads indicate N1ICD-positive nuclei; dotted line indicates the basement membrane. (D) Quantification of N1ICD-positive nuclei at P13 in WT and *K14Ift88* (number of animals for each genotype $n=2$). Data are represented as mean±s.d. $^{**}P<0.01$, $^{***}P<0.001$; Student's *t*-test.

support the notion that *Ift88* is directly involved in regulating the cell cycle (Ezratty et al., 2011; Robert et al., 2007). In this study, we have also found that ablation of *Ift88* has an overall impact on cell proliferation of basal CECs. However, in highly proliferating CE of 13-day-old *Ift88* cKO mice or during post-wounding conditions, absence of cilia had no effect on proliferation rates. These results suggest that at stages that require a high proliferation rate other pathways could override the effect of Ift88 on the cell cycle.

Cilia, corneal epithelium and Notch signaling

Surprisingly, ablation of *Ift88* and lack of cilia in K14-expressing cells of the CE did not affect the expression of target genes of cilia-mediated pathways, including the Hh and Wnt/β-catenin pathways. Moreover, reporter mouse lines indicated absence or low activity of these pathways during CE development and homeostasis (Fig. S2) in overall agreement with previous findings (Mukhopadhyay et al., 2006; Saika et al., 2004a; Zhang et al., 2015). By contrast, we found that ablation of *Ift88* in the CE downregulated the expression of the Notch pathway target genes. Furthermore, our results suggest that the cilium plays a role in the Notch pathway downstream of the ligand-receptor interaction in promoting the processing of Notch to generate NICD. Low levels of Notch due to cilia ablation could lead to a high rate of proliferation. This idea is consistent with previous studies showing that Notch activity negatively correlates with the proliferative status of the CE during repair and limits proliferation by inhibiting DeltaNp63 (Trp63) in the skin epidermis (Djalilian et al., 2008; Nguyen et al., 2006). However, it remains to be determined how the cilium compartment, or, more broadly, ciliary proteins, promote the processing of Notch.

Disruption of the Notch pathway in K14- and K15- (Krt15) expressing cells by ablation of the Notch1 receptor induces hyperplasia of basal CECs, cell fate change into skin-like tissue, and formation of an opaque plate at the center of the cornea (Vauclair et al., 2007). Although hyperplasia is consistent with the phenotype observed in the CE of the cilia-deficient mutants, we did not detect changes in cell fate or formation of corneal plaque (Fig. S3). These additional phenotypes could result from a more complete suppression of the Notch pathway activity in the *Notch1* knockout model. Alternatively, it was proposed that some of the Notch-related corneal phenotypes represent secondary effects caused by disruption of the Notch pathway in other tissues of the ocular surface. Supporting this possibility is the evidence that ectopic expression of the dominant-negative form of the transcriptional co-activator Maml1 in K14-expressing cells prevents the differentiation of conjunctival goblet cells (Zhang et al., 2013). As normal levels of Muc5ac are expressed at the conjunctiva of *K14Ift88* cKO mice, we conclude that goblet cell differentiation and function are not affected by the absence of cilia (Fig. S4).

In vitro data indicate that ablation of IFT components can accelerate cell cycle progression, which in turn could result in

Development (2016) 143, 2160-2171 doi:10.1242/dev.132704

reduced Notch activity (Ezratty et al., 2011; Robert et al., 2007). However, we showed that during postnatal development of the CE, ablation of Ift88 reduces Notch activity but does not affect proliferation, suggesting a role of cilia in the Notch pathway that is independent of cell proliferation. Although in the cornea we cannot exclude an indirect role of the cilium on the Notch pathway, studies on epidermis have shown the presence of the Notch3 receptor and presenilin 2, the γ-secretase component catalyzing NICD cleavage, along the cilium and at the bb area, respectively, suggesting a direct implication of the ciliary apparatus in the pathway (Ezratty et al., 2011). Components of the Notch pathways were also found at the cilium/bb apparatus in cultured retinal pigment epithelial cells. However, in this context depletion of ciliary proteins resulted in the upregulation of the Notch pathway (Leitch et al., 2014). In line with these results, disruption of IFT in the pancreas and in zebrafish tissues also abnormally increased Notch activity, suggesting a context-specific role of the cilium on Notch signaling (Cervantes et al., 2010; Leitch et al., 2014; Liu et al., 2014).

Cilia and tissue repair in the cornea

We previously showed that corneal endothelial cells assemble a cilium during cellular morphogenesis occurring during development and tissue repair (Blitzer et al., 2011). Surprisingly, CECs involved in the healing of CE do not assemble a cilium and their bbs do not appear to polarize (Fig. 4). Consistent with this evidence, wound closure of a circular abrasion of the CE in mice lacking *Ift88* in the CE occurs at rates similar to those observed in WT mice. We observed, however, that cilia reassemble after the wound closes and epithelial stratification begins. Taken together, these results support the idea that the CE cilium is not directly involved in early stages of CE wound healing, but rather that it plays a role in the CE stratification process.

MATERIALS AND METHODS

Mouse strains

Mouse strains *Ift88*^{tm1Bky}, here referred to as *Ift88*$^{fl/fl}$ (Haycraft et al., 2007), *Tg(KRT14-cre)1Amc/J* (Dassule et al., 2000), *Gt(ROSA)26Sor*$^{tm4(ACTB-tdTomato,-EGFP)Luo}$*/J*(*R26*$^{mT/mG}$) (Muzumdar et al., 2007), *Tg(TCF/Lef1-lacZ)34Efu/J*(*TopGAL*) (DasGupta and Fuchs, 1999) and *Gli1*^{tm2Alj}*/J* (*Gli1-LacZ*) (Bai et al., 2002) (Jackson Laboratories) were maintained on mixed C57BL/6, FVB and 129 genetic backgrounds. *Ift88* knockout mice were generated by crossing *KRT14-cre;Ift88*$^{fl/+}$ males with *Ift88*$^{fl/fl}$*R26*$^{mT/mG}$ female mice. Two- to three-month-old *KRT14-cre; Ift88*$^{fl/fl}$*;R26*$^{mT/mG}$ or *KRT14-cre; Ift88*$^{fl/fl}$ (here referred to as *K14Ift88* cKO) animals were used for the experiments unless otherwise specified. Littermates *Krt14*^{Cre}*Ift88*$^{fl/+}$ or *Ift88*$^{fl/fl}$ were used as controls. For genotyping primers, see Table S1. All animal procedures were performed in accordance with the guidelines and approval of the Institutional Animal Care and Use Committee at Icahn School of Medicine at Mount Sinai.

Immunohistochemistry, histology and electron microscopy

Enucleated eyes were directly embedded and frozen in optimal cutting temperature compound (OCT Tissue-Tek, Sakura). Sections (7 µm thick) were obtained and fixed with 4% paraformaldehyde (PFA) for 10 min at room temperature. For whole-mount preparations, eyes enucleated from mice of adult or young/embryonic age were fixed in 4% PFA at 4°C for 40 and 25 min, respectively. Corneas were then isolated and permeabilized with cold acetone for 5 min at −20°C.

Sections or whole-mounted corneas were blocked and permeabilized with 1% bovine serum albumin, 3% normal donkey serum (Jackson ImmunoResearch) and 0.1% TritonX-100 in PBS for 1 h at room temperature and processed as described previously (Blitzer et al., 2011; Saika et al., 2004b). Primary and secondary antibodies are listed in Table S2. For N1ICD, staining signals were visualized with Vectastain ABC Kit (Vector Laboratories) and TSA Plus Cyanine 3 System (PerkinElmer), according to manufacturers' instructions. Images were acquired with a Zeiss LSM510 confocal microscope. β-Galactosidase activity was detected by X-Gal staining performed on whole embryonic heads or enucleated eyes according to Chikama et al. (2005). Paraffin embedding and histology were performed following standard procedures.

For TEM and scanning electron microscopy (SEM), embryonic eyes or adult isolated corneas were fixed with 1% PFA and 3% glutaraldehyde in 0.1 M sodium cacodylate buffer, post-fixed with 1% osmium tetroxide, dehydrated through a graded series of ethanol and embedded in Epon (Electron Microscopy Sciences). Thin and ultrathin sections were cut on an ultramicrotome (Leica Ultracut UCT) and stained with uranyl acetate and lead citrate. Samples were observed using Hitachi H7650 or S4300 microscopes.

Ex vivo quantification of cell density and proliferation analysis

Confocal imaging was performed on whole eyes from *Ift88*$^{fl/fl}$*R26*$^{mT/mG}$ (red) and *K14*^{Cre}*Ift88*$^{fl/fl}$*;R26*$^{mT/mG}$ (green). Eyes were enucleated and stabilized with the cornea facing the glass bottom of a dish containing DMEM. The central epithelial layers were imaged using Zeiss LSM 510 confocal microscope. For each cornea, two 60-µm *z*-stacks of optical sections at 0.44-µm intervals were captured and analyzed using Zeiss LSM Image Browser software or Image J.

Mice (8 to 12 weeks old) received a single intraperitoneal injection of 50 mg/kg of 5-bromo-2-deoxyuridine (BrdU; Sigma-Aldrich) and were sacrificed after 2, 18 or 24 h. After fixation, corneas were incubated in 2 N HCl for 25 min at 37°C and processed for immunofluorescence. Cell proliferation was also assessed by immunostaining of PHH3. Nuclei were stained with Hoechst 33342. Six different *z*-stack images were obtained at 0.44-µm intervals for each area analyzed. Student's two-tailed test was performed using Excel, (Microsoft). Fisher's exact two-tailed test and ANOVA were performed using GraphPad Prism (GraphPad Software).

Wound-healing experiments

After anesthesia with Tribromoethanol-Avertin (Sigma), a 1.5 mm epithelial wound was induced using an Algerbrush (Ambler Surgical). To monitor wound size, fluorescein was applied to the wounded eye. After every procedure, eyes were treated with bacitracin antibiotic ointment (Fera). Eyes were photographed with a Leica L2 stereomicroscope at 0, 18, 24 h after wounding.

Quantitative RT-PCR

Corneal epithelial sheets from adult mice were mechanically peeled off enucleated eyes after overnight incubation in 4 mg/ml dispase II (Invitrogen) at 4°C. Total RNA was purified using the Absolutely RNA Micro Kit (Stratagene), quantified with a NanoDrop spectrophotometer (Thermo Scientific) and reverse transcribed (Superscript III First-Strand Synthesis System, Invitrogen) using oligo(dT) primers. Real-time PCR was performed using SYBR Green I Master (Roche) on LightCycler 480 (Roche). Quantification was performed using the 2−ΔΔCT method and *Gapdh* transcript as a reference. Measurements were performed in duplicate. Primer sequences and PCR conditions are listed in Table S3.

Western blot

Freshly isolated corneal epithelium was lysed in RIPA buffer (Sigma) supplemented with protease inhibitor cocktail (Roche). Standard western blot procedures were performed (Harlow and Lane, 1999) using antibodies listed in Table S2.

Acknowledgements

We thank Bradley Yoder and the UAB/HRFDCC (P30 DK074038) for providing the *Ift88*^{tm1Bky} mouse. We are grateful to Tom Tedeschi and Qing Liu for excellent technical assistance, and Yaseris Rosario-Peralta and Heather Bell for help with ultrastructural analysis. We thank all Mlodzik lab members and Winston W. Kao for helpful discussions, and Luca Gusella and Mario Wolosin for valuable comments on the manuscript. Confocal microscopy and image analysis was performed at the Icahn School of Medicine microscopy shared resource facility with the thoughtful guidance of Crystal Pristell.

Development (2016) 143, 2160-2171 doi:10.1242/dev.132704

Competing interests

The authors declare no competing or financial interests.

Author contributions

Conceptualization: L.G. and C.I.; investigation and methodology: L.G., E.R., R.E.G. and C.I.; visualization: L.G., E.R. and C.I.; writing of the original draft: L.G. and C.I.; writing, review and editing: L.G., E.R., and C.I.; supervision: C.I.

Funding

This work was supported by funding from the National Institutes of Health National Eye Institute [EY022639 to C.I.]; and a Dolly Green Special Scholar Award (to C.I.) and an unrestricted grant from Research to Prevent Blindness. Deposited in PMC for release after 12 months.

Supplementary information

Supplementary information available online at
http://dev.biologists.org/lookup/suppl/doi:10.1242/dev.132704/-/DC1

References

Bai, C. B., Auerbach, W., Lee, J. S., Stephen, D. and Joyner, A. L. (2002). Gli2, but not Gli1, is required for initial Shh signaling and ectopic activation of the Shh pathway. *Development* **129**, 4753-4761.

Berbari, N. F., O'Connor, A. K., Haycraft, C. J. and Yoder, B. K. (2009). The primary cilium as a complex signaling center. *Curr. Biol.* **19**, R526-R535.

Blitzer, A. L., Panagis, L., Gusella, G. L., Danias, J., Mlodzik, M. and Iomini, C. (2011). Primary cilia dynamics instruct tissue patterning and repair of corneal endothelium. *Proc. Natl. Acad. Sci. USA* **108**, 2819-2824.

Cervantes, S., Lau, J., Cano, D. A., Borromeo-Austin, C. and Hebrok, M. (2010). Primary cilia regulate Gli/Hedgehog activation in pancreas. *Proc. Natl. Acad. Sci. USA* **107**, 10109-10114.

Chen, S., Lee, B. H. and Bae, Y. (2014). Notch signaling in skeletal stem cells. *Calcif. Tissue Int.* **94**, 68-77.

Chikama, T.-I., Hayashi, Y., Liu, C.-Y., Terai, N., Terai, K., Kao, C. W.-C., Wang, L., Hayashi, M., Nishida, T., Sanford, P. et al. (2005). Characterization of tetracycline-inducible bitransgenic Krt12 rtTA/+/tet-O-LacZ mice. *Invest. Ophthalmol. Vis. Sci.* **46**, 1966-1972.

Cotsarelis, G., Cheng, S.-Z., Dong, G., Sun, T.-T. and Lavker, R. M. (1989). Existence of slow-cycling limbal epithelial basal cells that can be preferentially stimulated to proliferate: implications on epithelial stem cells. *Cell* **57**, 201-209.

Croyle, M. J., Lehman, J. M., O'Connor, A. K., Wong, S. Y., Malarkey, E. B., Iribarne, D., Dowdle, W. E., Schoeb, T. R., Verney, Z. M., Athar, M. et al. (2011). Role of epidermal primary cilia in the homeostasis of skin and hair follicles. *Development* **138**, 1675-1685.

DasGupta, R. and Fuchs, E. (1999). Multiple roles for activated LEF/TCF transcription complexes during hair follicle development and differentiation. *Development* **126**, 4557-4568.

Dassule, H. R., Lewis, P., Bei, M., Maas, R. and McMahon, A. P. (2000). Sonic hedgehog regulates growth and morphogenesis of the tooth. *Development* **127**, 4775-4785.

Davanger, M. and Evensen, A. (1971). Role of the pericorneal papillary structure in renewal of corneal epithelium. *Nature* **229**, 560-561.

Djalilian, A. R., Namavari, A., Ito, A., Balali, S., Afshar, A., Lavker, R. M. and Yue, B. Y. (2008). Down-regulation of Notch signaling during corneal epithelial proliferation. *Mol. Vis.* **14**, 1041-1049.

Douvaras, P., Mort, R. L., Edwards, D., Ramaesh, K., Dhillon, B., Morley, S. D., Hill, R. E. and West, J. D. (2013). Increased corneal epithelial turnover contributes to abnormal homeostasis in the Pax6(+/–) mouse model of aniridia. *PLoS ONE* **8**, e71117.

Ezratty, E. J., Stokes, N., Chai, S., Shah, A. S., Williams, S. E. and Fuchs, E. (2011). A role for the primary cilium in Notch signaling and epidermal differentiation during skin development. *Cell* **145**, 1129-1141.

Friedenwald, J. S. and Buschke, W. (1944). Some factors concerned in the mitotic and wound-healing activities of the corneal epithelium. *Trans. Am. Ophthalmol. Soc.* **42**, 371-383.

Goetz, S. C. and Anderson, K. V. (2010). The primary cilium: a signalling centre during vertebrate development. *Nat. Rev. Genet.* **11**, 331-344.

Guentchev, M. and McKay, R. D. G. (2006). Notch controls proliferation and differentiation of stem cells in a dose-dependent manner. *Eur. J. Neurosci.* **23**, 2289-2296.

Harlow, E. and Lane, D. (1999). *Using Antibodies: A Laboratory Manual.* Cold Spring Harbor, NY: Cold Spring Harbor Laboratory Press.

Haycraft, C. J., Zhang, Q., Song, B., Jackson, W. S., Detloff, P. J., Serra, R. and Yoder, B. K. (2007). Intraflagellar transport is essential for endochondral bone formation. *Development* **134**, 307-316.

Huang, D., Wang, J., Lin, C. P., Puliafito, C. A. and Fujimoto, J. G. (1991). Micron-resolution ranging of cornea anterior chamber by optical reflectometry. *Lasers Surg. Med.* **11**, 419-425.

Kopan, R. and Ilagan, M. X. G. (2009). The canonical Notch signaling pathway: unfolding the activation mechanism. *Cell* **137**, 216-233.

Kurpakus, M. A., Maniaci, M. T. and Esco, M. (1994). Expression of keratins K12, K4 and K14 during development of ocular surface epithelium. *Curr. Eye Res.* **13**, 805-814.

Kuwabara, T., Perkins, D. G. and Cogan, D. G. (1976). Sliding of the epithelium in experimental corneal wounds. *Invest. Ophthalmol.* **15**, 4-14.

Leitch, C. C., Lodh, S., Prieto-Echague, V., Badano, J. L. and Zaghloul, N. A. (2014). Basal body proteins regulate Notch signaling through endosomal trafficking. *J. Cell Sci.* **127**, 2407-2419.

Liu, Y. P., Tsai, I.-C., Morleo, M., Oh, E. C., Leitch, C. C., Massa, F., Lee, B.-H., Parker, D. S., Finley, D., Zaghloul, N. A. et al. (2014). Ciliopathy proteins regulate paracrine signaling by modulating proteasomal degradation of mediators. *J. Clin. Invest.* **124**, 2059-2070.

Ma, A., Zhao, B., Boulton, M. and Albon, J. (2011). A role for Notch signaling in corneal wound healing. *Wound Repair Regen.* **19**, 98-106.

MacRae, D. W., Howard, R. O., Albert, D. M. and Hsia, Y. E. (1972). Ocular manifestations of the Meckel syndrome. *Arch. Ophthalmol.* **88**, 106-113.

Mukhopadhyay, M., Gorivodsky, M., Shtrom, S., Grinberg, A., Niehrs, C., Morasso, M. I. and Westphal, H. (2006). Dkk2 plays an essential role in the corneal fate of the ocular surface epithelium. *Development* **133**, 2149-2154.

Muzumdar, M. D., Tasic, B., Miyamichi, K., Li, L. and Luo, L. (2007). A global double-fluorescent Cre reporter mouse. *Genesis* **45**, 593-605.

Nakamura, T., Ohtsuka, T., Sekiyama, E., Cooper, L. J., Kokubu, H., Fullwood, N. J., Barrandon, Y., Kageyama, R. and Kinoshita, S. (2008). Hes1 regulates corneal development and the function of corneal epithelial stem/progenitor cells. *Stem Cells* **26**, 1265-1274.

Nguyen, B.-C., Lefort, K., Mandinova, A., Antonini, D., Devgan, V., Della Gatta, G., Koster, M. I., Zhang, Z., Wang, J., Tommasi di Vignano, A. et al. (2006). Cross-regulation between Notch and p63 in keratinocyte commitment to differentiation. *Genes Dev.* **20**, 1028-1042.

Nishida, K., Kinoshita, S., Ohashi, Y., Kuwayama, Y. and Yamamoto, S. (1995). Ocular surface abnormalities in aniridia. *Am. J. Ophthalmol.* **120**, 368-375.

Park, T. J., Mitchell, B. J., Abitua, P. B., Kintner, C. and Wallingford, J. B. (2008). Dishevelled controls apical docking and planar polarization of basal bodies in ciliated epithelial cells. *Nat. Genet.* **40**, 871-879.

Pei, Y. F. and Rhodin, J. A. (1971). Electron microscopic study of the development of the mouse corneal epithelium. *Invest. Ophthalmol.* **10**, 811-825.

Robert, A., Margall-Ducos, G., Guidotti, J.-E., Bregerie, O., Celati, C., Brechot, C. and Desdouets, C. (2007). The intraflagellar transport component IFT88/polaris is a centrosomal protein regulating G1-S transition in non-ciliated cells. *J. Cell Sci.* **120**, 628-637.

Rosenbaum, J. L. and Witman, G. B. (2002). Intraflagellar transport. *Nat. Rev. Mol. Cell Biol.* **3**, 813-825.

Saika, S., Muragaki, Y., Okada, Y., Miyamoto, T., Ohnishi, Y., Ooshima, A. and Kao, W. W.-Y. (2004a). Sonic hedgehog expression and role in healing corneal epithelium. *Invest. Ophthalmol. Vis. Sci.* **45**, 2577-2585.

Saika, S., Okada, Y., Miyamoto, T., Yamanaka, O., Ohnishi, Y., Ooshima, A., Liu, C.-Y., Weng, D. and Kao, W. W.-Y. (2004b). Role of p38 MAP kinase in regulation of cell migration and proliferation in healing corneal epithelium. *Invest. Ophthalmol. Vis. Sci.* **45**, 100-109.

Schmidt, K. N., Kuhns, S., Neuner, A., Hub, B., Zentgraf, H. and Pereira, G. (2012). Cep164 mediates vesicular docking to the mother centriole during early steps of ciliogenesis. *J. Cell Biol.* **199**, 1083-1101.

Schroeter, E. H., Kisslinger, J. A. and Kopan, R. (1998). Notch-1 signalling requires ligand-induced proteolytic release of intracellular domain. *Nature* **393**, 382-386.

Sharma, N., Berbari, N. F. and Yoder, B. K. (2008). Ciliary dysfunction in developmental abnormalities and diseases. *Curr. Top. Dev. Biol.* **85**, 371-427.

Stepp, M. A., Gibson, H. E., Gala, P. H., Sta. Iglesia, D. D., Pajoohesh-Ganji, A., Pal-Ghosh, S., Brown, M., Aquino, C., Schwartz, A. M., Goldberger, O. et al. (2002). Defects in keratinocyte activation during wound healing in the syndecan-1-deficient mouse. *J. Cell Sci.* **115**, 4517-4531.

Stepp, M. A., Zieske, J. D., Trinkaus-Randall, V., Kyne, B. M., Pal-Ghosh, S., Tadvalkar, G. and Pajoohesh-Ganji, A. (2014). Wounding the cornea to learn how it heals. *Exp. Eye Res.* **121**, 178-193.

Tanifuji-Terai, N., Terai, K., Hayashi, Y., Chikama, T.-I. and Kao, W. W.-Y. (2006). Expression of keratin 12 and maturation of corneal epithelium during development and postnatal growth. *Invest. Ophthalmol. Vis. Sci.* **47**, 545-551.

Thoft, R. A. and Friend, J. (1983). The X, Y, Z hypothesis of corneal epithelial maintenance. *Invest. Ophthalmol. Vis. Sci.* **24**, 1442-1443.

Tseng, H., Matsuzaki, K. and Lavker, R. M. (1999). Basonuclin in murine corneal and lens epithelia correlates with cellular maturation and proliferative ability. *Differentiation* **65**, 221-227.

Vauclair, S., Majo, F., Durham, A.-D., Ghyselinck, N. B., Barrandon, Y. and Radtke, F. (2007). Corneal epithelial cell fate is maintained during repair by Notch1 signaling via the regulation of vitamin A metabolism. *Dev. Cell* **13**, 242-253.

Wood, C. R., Huang, K., Diener, D. R. and Rosenbaum, J. L. (2013). The cilium secretes bioactive ectosomes. *Curr. Biol.* **23**, 906-911.

Development (2016) 143, 2160-2171 doi:10.1242/dev.132704

Xiong, L., Woodward, A. M. and Argüeso, P. (2011). Notch signaling modulates MUC16 biosynthesis in an in vitro model of human corneal and conjunctival epithelial cell differentiation. *Invest. Ophthalmol. Vis. Sci.* **52**, 5641-5646.

Zagon, I. S., Sassani, J. W. and McLaughlin, P. J. (1999). Cellular dynamics of corneal wound re-epithelialization in the rat. II. DNA synthesis of the ocular surface epithelium following wounding. *Brain Res.* **839**, 243-252.

Zhang, Y., Lam, O., Nguyen, M.-T. T., Ng, G., Pear, W. S., Ai, W., Wang, I.-J., Kao, W. W.-Y. and Liu, C.-Y. (2013). Mastermind-like transcriptional co-activator-mediated Notch signaling is indispensable for maintaining conjunctival epithelial identity. *Development* **140**, 594-605.

Zhang, Y., Yeh, L.-K., Zhang, S., Call, M., Yuan, Y., Yasunaga, M., Kao, W. W.-Y. and Liu, C.-Y. (2015). Wnt/beta-catenin signaling modulates corneal epithelium stratification via inhibition of Bmp4 during mouse development. *Development* **142**, 3383-3393.

Zieske, J. D. (2004). Corneal development associated with eyelid opening. *Int. J. Dev. Biol.* **48**, 903-911.